Electronic Supplementary Information

Dendron-mediated control over self-assembly of chlorophyll rosettes into columnar vs discrete aggregates

Ryo Kudo,[a] Hiroki Hanayama,[b] Balaraman Vedhanarayanan,[c] Hitoshi Tamiaki,[d] Nobuyuki Hara,[d,e] Sarah E. Rogers,[f] Martin J. Hollamby,[g] Biplab Manna,[h] Koji Harano,[h] and Shiki Yagai[b,i*]

[a]*Division of Advanced Science and Engineering, Graduate School of Engineering, Chiba University, 1-33 Yayoi-cho, Inage-ku, Chiba 263-8522, Japan.*

[b]*Department of Applied Chemistry and Biotechnology, Graduate School of Engineering, Chiba University, 1-33 Yayoi-cho, Inage-ku, Chiba 263-8522, Japan.*

[c]*Department of Chemistry, Faculty of Engineering and Technology, SRM Institute of Science and Technology, Kattankulathur, Chengalpattu 603 203, Tamil Nadu, India.*

[d]*Graduate School of Life Sciences, Ritsumeikan University, Kusatsu, Shiga 525-8577, Japan.*

[e]*Department of Chemistry, College of Humanities & Sciences, Nihon University, Setagaya-ku, Tokyo 156-8550, Japan.*

[f]*ISIS Pulsed Neutron Source, Rutherford Appleton Laboratory, Didcot, OX11 0QX, U.K.*

[g]*Department of Chemistry, School of Chemical and Physical Sciences, Keele University, Keele, Staffordshire ST55BG, U.K.*

[h]*Center for Basic Research on Materials, National Institute for Materials Science, 1-1 Namiki, Tsukuba, Ibaraki 305-0044, Japan.*

[i]*Institute for Advanced Academic Research (IAAR), Chiba University, 1-33 Yayoi-cho, Inage-ku, Chiba 263-8522, Japan.*

Email: yagai@faculty.chiba-u.jp

Table of contents

1. General

Materials and methods

ChG2 and **ChG3** were synthesized by following the procedure outlined in **Scheme S1**. All commercially available reagents and solvents were of reagent-grade quality and used without further purification. Spectroscopic-grade solvents were employed for spectroscopic measurements without additional purification steps. ^{1}H and ^{13}C NMR spectra were recorded on Bruker DPX 300 spectrometer and JEOL JMN-ECA500 NMR spectrometer. ^{1}H NMR chemical shifts are reported in parts per million (ppm, δ), referenced to tetramethylsilane (TMS) as internal standard at 0.00 ppm. Signal multiplicities are indicated as s (singlet), d (doublet), t (triplet), q (quartet), m (multiplet), and brs (broad singlet). ^{13}C NMR chemical shifts were referenced to the $CDCl_3$ solvent signal at 77.16 ppm. Electrospray ionization mass spectrometry (ESI-MS) spectrum measurement was conducted on Thermo Scientific Exactive. UV/Vis absorption spectra were measured using JASCO V660 and V760 spectrophotometers equipped with JASCO ETCS-761 temperature-control unit. Screw-capped quartz cuvettes with optical path length of 1.0 cm and 1.0 mm were used. Circular dichroism (CD) spectra were recorded on JASCO J840 spectropolarimeter equipped with a JASCO PTC-423L temperature controller. CD measurements were performed using a screw-capped quartz cuvettes with optical path length of 1.0 cm and 1.0 mm.

Atomic force microscopy (AFM)

AFM imaging was conducted under ambient conditions using a Multimode 8 Nanoscope V (Bruker) in Peak Force Tapping (ScanAsyst) mode. Silicon cantilevers (SCANASYSTAIR) with a nominal spring constant of 0.4 N/m and frequency of 70 kHz (nominal value, Bruker, Japan) were used. The samples were prepared by spin-coating (3000 rpm, 1 min) 10 μL of supramolecular polymer solution onto freshly cleaved highly oriented pyrolytic graphite (HOPG, 5 mm × 5 mm) at 293 K. Images were processed using NanoScope Analysis 3.00 software.

Transmission electron microscopy (TEM)

TEM was carried out on Talos F200X G2 (Thermo Fisher Scientific) operated at an accelerating voltage of 80 kV under 5×10^{-6} Pa in the specimen column. TEM images were recorded at an underfocus condition (defocus value: 1–2 μm) with an exposure time of 1.0 sec on Ceta-D camera. TEM specimen of **ChG2** was prepared by drop-casting sample solution (ca. 10 μL) onto thin carbon-coated copper grid (SHR-C075, Okenshoji Co., Ltd.) followed by drying in vacuum. Specimen of **ChG3** was prepared by spin-coating (3000 rpm, 5 min) 5 μL of sample solution onto SHR-C075. All images were processed using Gaussian blur filter using ImageJ 1.54f software.[S1]

TEM image simulation was carried out using FH electron optics ELBIS software by parallelized computation using a graphics processing unit.[S2] The parameters for simulation were set to be

acceleration voltage = 80 kV, spherical aberration constant C_s = 2 mm, defocus value = −1.5 mm (underfocus).

Small-angle X-ray scattering (SAXS) measurements

SAXS measurements were conducted at BL-10C at the Photon Factory of the High Energy Accelerator Research Organization (KEK) in Tsukuba, Japan. Sample solutions were placed in specialized cells featuring a stainless-steel frame and 20-μm-thick quartz glass windows, with a 1.25-mm optical path length. Temperature was maintained at room temperature. The experimental setup using X-ray wavelength of 1.5 Å and a sample-detector distance of 1029 mm (calibrated using silver behenate) allowed for a detectable Q-range spanning from 0.1 to 5.9 nm^{-1}. Data were collected in 60 frames, each with an exposure time of 10 s. No signs of radiation damage were observed, allowing the frames to be averaged, resulting in a total integration time of 600 s. Scattering data were captured using a DECTRIS PILATUS3 2M detector and subsequently converted from 2D to 1D scattering intensity profiles [$I(Q)$ versus Q] through radial averaging. The resulting intensity data were normalized with water as a reference standard. The background, attributed to both solvent and cell, was subtracted to yield absolute scattering intensities, reported as $I(Q)$ in cm^{-1}. All data reduction were executed using the SAngler software package.[S3]

Small-angle neutron scattering (SANS) measurements

SANS measurements were carried out on the SANS2D beamline at the ISIS Neutron and Muon source, Rutherford Appleton Laboratory, UK. Two samples were studied: 3×10^{-4} M solutions of **ChG2** and **ChG3** in methylcyclohexane (MCH)-d_{14} (Apollo Scientific, 99.5% D). Samples were measured in 2 mm pathlength quartz banjo cells and a thermostatted sample changer provided temperature control. A 12-mm beam and two offset detectors with sample-to-detector distances of 2.36 and 4.00 m respectively were used, providing a detectable Q range of 0.005–0.9 $Å^{-1}$ for the merged datasets. Measurement times were approx. 30 min. Raw data were radially averaged and corrected for transmission, background and detector efficiency using Mantid.[S4] Data were placed on an absolute scale (cm^{-1}) using the scattering from a standard sample (a solid blend of hydrogenous and perdeuterated polystyrene).

Model fitting of SAXS and SANS data

In all cases, SANS and SAXS data were fitted simultaneously with shared parameters as detailed below. All fitting approaches use as their basis a model representing a core-shell cylinder with no end caps, in line with AFM images. Specifically, in SasView, the model used was “core_shell_bicelle”,[S5] with the face thickness set to zero. The scattered intensity of the core-shell cylinder is calculated using Equations S1 and S2.

$$I_{(q,\alpha)} = \frac{scale}{V_{total}} F^2(q,\alpha)\sin(\alpha) + I_{bkg} \quad \text{(S1)}$$

$$F(q,\alpha) = \left[(\rho_{core} - \rho_{shell})V_{core}\frac{2J_1(QR_{core}\sin\alpha)}{QR_{core}\sin\alpha}\frac{\sin(QL\cos\alpha/2)}{QL\cos\alpha/2}\right.$$
$$\left. + (\rho_{shell} - \rho_{\text{solvent}})V_{total}\frac{2J_1(Q(R_{core}+\delta_{shell})\sin\alpha)}{Q(R_{core}+\delta_{shell})\sin\alpha}\frac{\sin(QL\cos\alpha/2)}{QL\cos\alpha/2}\right] \quad \text{(S2)}$$

In the above, α is the angle between the Q vector and the cylinder axis "*scale*" is the volume fraction, I_{bkg} is a flat background, which mostly accounts for incoherent scattering originating from the H content of the samples, V_{total} is the total volume of the core-shell cylinder, V_{core} is the volume of the core, R_{core} is the core radius, δ_{shell} is the shell thickness, L is the cylinder length, and ρ_{core}, ρ_{shell} and ρ_{solvent} are the scattering length densities of the core, shell and solvent, respectively.

Scattering length densities, scale and approach to analysis

The scattering length density for MCH-d_{14} was calculated as $\rho_{\text{solvent,SANS}} = 6.6 \times 10^{-6}$ Å^{-2} and $\rho_{\text{solvent,SAXS}} = 7.45 \times 10^{-6}$ Å^{-2}. Following our work on related derivative,[S6] the "core" has been taken to include the barbituric acid moiety, chlorin moiety, plus dendritic linkers and trioxyphenyl units. The shell then comprises just the *n*-$C_{12}H_{25}$ chains. Using ACD Chem Sketch to approximate the density as 1.54 ± 0.1 g mL^{-1} and 1.53 ± 0.1 g mL^{-1} for these "core" sections of **ChG2** ($C_{57}H_{46}N_6O_{14}$) and **ChG3** ($C_{85}H_{64}N_6O_{24}$) respectively, the scattering length densities were found to be $\rho_{\text{core,SANS}} = 3.07 \times 10^{-6}$ Å^{-2} and $\rho_{\text{core,SAXS}} = 13.7 \times 10^{-6}$ Å^{-2} for **ChG2** and $\rho_{\text{core,SANS}} = 3.11 \times 10^{-6}$ Å^{-2} and $\rho_{\text{core,SAXS}} = 13.6 \times 10^{-6}$ Å^{-2} for **ChG3**. By the same method, the density of the full **ChG2** and **ChG3** derivatives were found to be 1.09 ± 0.1 g mL^{-1} and 1.05 ± 0.1 g mL^{-1} and therefore for c = 300 μM, *scale* = 5.66×10^{-4} for **ChG2** and *scale* = 1.02×10^{-3} for **ChG3**. These values were all fixed in the analysis.

In the past work, we have at times allowed ρ_{shell} to float, while constraining δ_{shell}, as the correlation between those parameters can make the fit unstable, yielding unrealistic parameters if both are allowed to float. Here, that approach was trialed, but it was found that the level of solvent penetration was low – in line with the denser alkyl regions on the outside of these assemblies due to their dendritic structures. As such, here we have instead held ρ_{shell} constant (at $\rho_{\text{shell,SANS}} = -0.37 \times 10^{-6}$ Å^{-2} and $\rho_{\text{shell,SAXS}} = 7.3 \times 10^{-6}$ Å^{-2} and allowed δ_{shell} to float. The fitted values of δ_{shell} then represent the full extent of the alkyl region unpenetrated by solvent. The fitted values of δ_{shell} = 11–12 Å are a little lower than that approximated by Tanford's formula for the length of a fully outstretched alkyl chain (16.7 Å),[S6] which could indicate that not all chains point directly outwards, or perhaps that the very outside of the shell has considerable solvent penetration.

The analysis therefore proceeded as follows. For **ChG2**, R_{core} and δ_{shell} were floated, but constrained to the same value for SAXS and SANS datasets. Given evidence from AFM measurements,

and the clear I(Q) ~ Q^{-1} dependency in both datasets persisting throughout the low Q region, L was fixed at 1000 Å (= 100 nm). For **ChG3**, R_{core}, δ_{shell} and L were all floated and constrained to the same value for SAXS and SANS datasets. The rationale for this is explained in the main text, alongside the analysis results. In both cases, other values were fixed as described above.

As noted in the MS, there is good agreement between model and data in all but the SAXS data for **ChG2**. There, a maximum at Q ~0.28 $Å^{-1}$ (corresponding d ~2.2 nm) is visible in the SAXS but not in the SANS (for which the agreement with analysis is excellent). More complex fitting methods, for example using an elliptical rather than circular core, were trailed but failed to match both SAXS and SANS results. It is at present difficult to understand the origin of this phenomenon, although it is notable that 2.2 nm is near the height of individual rosettes (*e.g.* SAXS/SANS and AFM analysis of **ChG3**). One suggestion is therefore that the maximum may originate from a repeating distance between chlorin moieties within the fibers, which then mask the expected oscillations for the core-shell model in the SAXS. If that is the case, then taken with the AFM evidence of a ~9.5 nm pitch and a clockwise rotation upon stacking, it may be that each clockwise turn is of order 90°, yielding ~4 turns per visible pitch. The rationale for the lack of its appearance in the SANS would then be the far less well-defined repeating distance between alkyl regions – due to the twist and their potential for interpenetration (that the chlorin moieties cannot achieve).

2. Synthesis and characterization

ChG2 and **ChG3** were synthesized by following the procedure as shown in Scheme S1. Synthesis of compounds **1**,[S7] **2**,[S8] and **3**[S8] were reported previously.

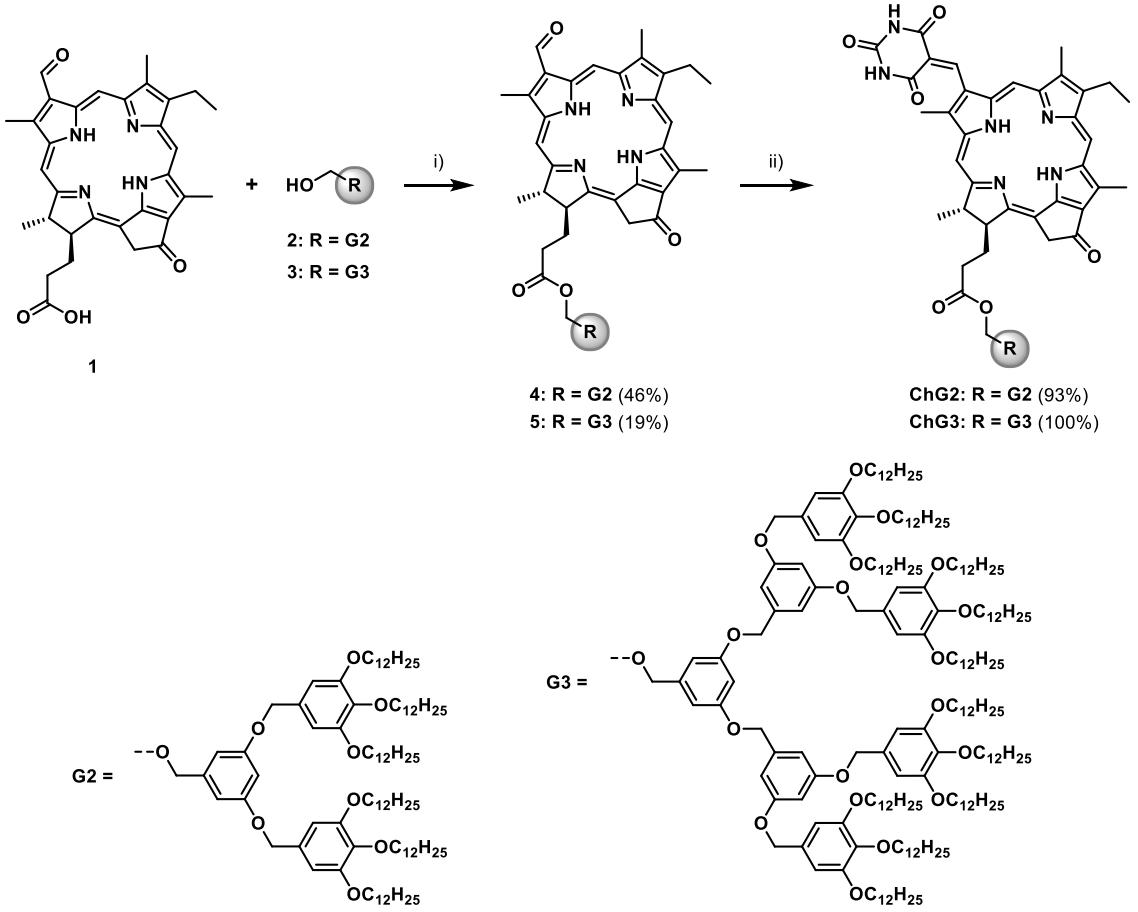

Scheme S1 Synthesis of compounds **ChG2** and **ChG3**. i) 1-(3-Dimethylaminopropyl)-3-ethylcarbodiimide hydrochloride (EDC·HCl), *N*,*N*'-dimethyl-4-aminopyridine (DMAP), CH_2Cl_2, 0 °C → 25 °C; ii) barbituric acid, MeOH/THF (1:7 v/v) for **ChG2**, EtOH/THF (1:1 v/v) for **ChG3**, reflux.

Compound 4

Compound **1** (52 mg, 97 μmol), **2** (184 mg, 139 μmol) and DMAP (23 mg, 190 μmol) were dissolved in 25 mL of $CHCl_2$ in a 300 mL eggplant flask at 0 °C. To this mixture, EDC·HCl (56 mg, 290 μmol) was added and stirred for 6 h at 25 °C. The mixture was then diluted with CH_2Cl_2 and washed with H_2O and then brine. The organic layer separated was dried over Na_2SO_4 and then evaporated to dryness under reduced pressure. The resulting solid was purified by column chromatography over silica gel (eluent: *n*-hexane/AcOEt = 5:1) to give compound **4** as dark reddish solid (87 mg, 46% yield). ^{1}H NMR (500 MHz, $CDCl_3$): δ = 11.54 (s, 1H), 10.31 (s, 1H), 9.62 (s, 1H), 8.83 (s, 1H), 6.56–6.52 (m, 5H), 6.51 (d, J = 2.1 Hz, 2H), 5.32 (d, J = 19.9 Hz, 1H), 5.16 (d, J = 19.9 Hz, 1H), 5.02 (d, J = 12.5 Hz, 1H), 4.97 (d, J = 12.5 Hz, 1H), 4.83 (s, 4H), 4.61–4.54 (m, 1H), 4.37–4.34 (m, 1H), 3.97–3.88 (m,

12H), 3.76–3.71 (m, 8H), 3.32 (s, 3H), 2.80–2.60 (m, 2H), 2.40–2.27 (m, 2H), 1.82 (d, J = 7.3 Hz, 3H), 1.74–1.68 (m, 15H), 1.46–1.23 (m, 108H), 0.89–0.84 (m, 18H), 0.13 (brs, 1H), −2.07 (brs, 1H). ^{13}C NMR (126 MHz, $CDCl_3$): δ = 195.97, 188.35, 172.74, 169.80, 160.09, 155.24, 153.28, 148.58, 144.98, 140.70, 139.86, 137.65, 137.90, 137.83, 134.09, 131.88, 131.42, 130.18, 129.36, 107.16, 107.11, 106.20, 105.28, 103.41, 101.70, 99.99, 94.94, 73.43, 70.55, 69.07, 66.33, 52.22, 49.43, 48.23, 31.97, 31.11, 30.36, 29.80, 29.73, 29.69, 29.67, 29.44. HRMS (ESI): *m/z* calcd for $C_{125}H_{194}N_4O_{12}$ $[M+H]^+$ 1944.4766, found 1944.4752.

Compound 5

Compound **1** (127 mg, 237 μmol), **3** (340 mg, 115 μmol) and DMAP (42 mg, 344 μmol) were dissolved in 15 mL of $CHCl_2$ in a 250 mL eggplant flask at 0 °C. To this mixture, EDC·HCl (109 mg, 569 μmol) was added and stirred for 15 h at 25 °C. The reaction was monitored by TLC (*n*-hexane/$CHCl_2$ = 1:4). The mixture was evaporated to dryness under reduced pressure and then purified by GPC (eluent: $CHCl_3$) to give compound **5** as dark reddish solid (76 mg, 19% yield). ^{1}H NMR (500 MHz, $CDCl_3$): δ = 11.52 (s, 1H), 10.29 (s, 1H), 9.59 (s, 1H), 8.81 (s, 1H), 6.64 (d, J = 2.1 Hz, 4H), 6.57 (s, 8H), 6.55 (t, J = 2.2 Hz, 1H), 6.53 (t, J = 2.1 Hz, 2H), 6.51 (d, J = 2.1 Hz, 2H), 5.31 (d, J = 19.8 Hz, 1H), 5.13 (d, J = 19.8 Hz, 1H), 5.01 (d, J = 12.5 Hz, 1H), 4.92 (d, J = 12.5 Hz, 1H), 4.90 (s, 4H), 4.84 (s, 8H), 4.56–4.54 (m, 1H), 4.38–4.36 (m, 1H), 3.94–3.90 (m, 24H), 3.73–3.68 (m, 8H), 3.31 (s, 3H), 2.80–2.63 (m, 2H), 2.44–2.28 (m, 2H), 1.82–1.73 (m, 30H), 1.46–1.23 (m, 220H), 0.89–0.84 (m, 36H), −0.13 (brs, 1H), −2.08 (brs, 1H). ^{13}C NMR (126 MHz, $CDCl_3$): δ = 195.88, 188.32, 172.70, 169.80, 161.76, 160.20, 160.05, 155.28, 153.32, 152.84, 152.51, 148.61, 145.00, 140.70, 139.89, 138.99, 138.37, 138.06, 138.00, 137.86, 134.14, 131.91, 131.51, 130.17, 129.42, 107.19, 106.73, 106.41, 106.30, 103.42, 101.78, 101.51, 100.04, 94.92, 73.45, 70.57, 70.08, 69.14, 66.28, 52.26, 49.44, 48.23, 31.97, 31.94, 31.19, 30.39, 29.79, 29.73, 29.68, 29.46, 29.45, 29.42, 29.39, 29.23, 26.18, 26.15, 26.00, 23.47, 22.72, 22.70, 19.50, 17.41, 14.13, 12.17, 11.29. HRMS (ESI): *m/z* calcd for $C_{225}H_{362}N_4O_{22}$ $[M+H]^+$ 3473.7404, found 3473.7405.

ChG2

A mixture of **4** (80 mg, 41 μmol) and barbituric acid (27 mg, 210 μmol) in 1:7 MeOH/THF mixture (8 mL) was refluxed for 17 h. The reaction mixture was cooled to 25 °C, and the resulting precipitates were collected by filtration and washed with hot EtOH repeatedly. The residual solid was further purified by reprecipitation from a mixture of $CHCl_3$ and EtOH to give pure **ChG2** as deep green solids (79 mg, 93% yield). ^{1}H NMR (400 MHz, $CDCl_3$): δ = 10.08 (s, 1H), 9.57 (s, 1H), 9.23 (s, 1H), 8.75 (s, 1H), 8.32 (s, 1H), 8.21 (s, 1H), 6.56 (s, 4H), 6.55 (s, 3H), 5.28 (d, J = 19.9 Hz, 1H), 5.13 (d, J = 19.9 Hz, 1H), 5.02 (d, J = 12.4 Hz, 1H), 4.97 (d, J = 12.4 Hz, 1H), 4.84 (s, 4H), 4.52 (dq, J = 7.1 Hz, 1.6 Hz, 1H), 4.36 (td, J = 8.4 Hz, 2.1 Hz, 1H), 3.93–3.89 (m, 12H), 3.71–3.69 (m, 5H), 3.12 (s, 3H), 3.24 (s, 3H), 2.76–2.60 (m, 2H), 2.36–2.27 (m, 2H), 1.80 (d, J = 7.3 Hz, 3H), 1.77–1.69 (m, 15H), 1.46–1.23 (m, 108H), 0.89–0.84 (m, 18H), 0.10 (brs, 1H), −1.82 (brs, 1H). ^{13}C NMR (126 MHz, $CDCl_3$): δ = 195.86, 172.78, 170.46, 162.04, 161.30, 160.14, 159.35, 154.57, 153.29, 151.97, 151.80,

148.82, 148.75, 145.14, 140.02, 139.40, 138.48, 138.04, 137.99, 136.65, 135.23, 131.58, 131.48, 130.67, 129.76, 120.04, 107.20, 107.15, 106.34, 103.80, 101.80, 97.54, 95.02, 73.47, 70.59, 69.14, 66.35, 52.05, 49.60, 48.12, 31.96, 31.14, 30.35, 29.77, 29.76, 29.71, 29.66, 29.44, 29.42, 29.37, 26.15, 26.12, 23.33, 22.71, 22.70, 19.44, 17.37, 14.53, 14.12, 12.09, 11.29. HRMS (ESI): *m/z* calcd for $C_{129}H_{196}N_6O_4$ $[M+H]^+$ 2054.4882, found 2054.4834.

ChG3

A mixture of **5** (58 mg, 17 μmol) and barbituric acid (87 mg, 680 μmol) in 1:1 EtOH/THF mixture (3 mL) was refluxed for 12 h. The reaction mixture was cooled to 25 °C, and the resulting precipitates were collected by filtration and washed with hot EtOH repeatedly. The residual solid was further purified by reprecipitation from a $CHCl_3$-MeOH mixture to give pure **ChG3** as deep green solids (63 mg, 100% yield). ^{1}H NMR (500 MHz, $CDCl_3$): δ = 10.07 (s, 1H), 9.54 (s, 1H), 9.22 (s, 1H), 8.74 (s, 1H), 8.38 (s, 1H), 8.24 (s, 1H), 6.66 (d, J = 1.9 Hz, 4H), 6.58–6.53 (m, 13H), 5.28 (d, J = 19.7 Hz, 1H), 5.23 (d, J = 19.7 Hz, 1H), 5.02 (d, J = 12.3 Hz, 1H), 4.94 (d, J = 12.3 Hz, 1H), 4.91 (s, 4H), 4.86 (s, 8H), 4.52–4.50 (m, 1H), 4.34–4.32 (m, 1H), 3.94–3.91 (m, 24H), 3.73–3.66 (m, 5H), 3.29 (s, 3H), 3.22 (s, 3H), 2.72–2.61 (m, 2H), 2.39–2.28 (m, 2H), 1.80–1.67 (m, 30H), 1.45–1.23 (m, 216H), 0.88–0.84 (m, 36H), 0.07 (brs, 1H), −1.84 (brs, 1H). ^{13}C NMR (126 MHz, $CDCl_3$): δ = 195.87, 172.76, 170.47, 161.99, 161.31, 160.20, 160.07, 159.33, 154.63, 153.32, 152.84, 152.01, 151.70, 148.83, 148.64, 145.17, 140.03, 139.42, 139.02, 138.50, 138.05, 136.69, 135.28, 131.58, 131.54, 130.71, 129.76, 120.06, 107.27, 107.18, 106.75, 106.45, 106.33, 103.84, 101.83, 101.57, 97.57, 95.03, 73.47, 70.60, 70.10, 69.16, 66.33, 52.05, 49.60, 48.14, 31.97, 31.95, 31.17, 30.39, 29.79, 29.78, 29.73, 29.68, 29.47, 29.43, 29.39, 26.18, 26.16, 23.48, 23.36, 22.73, 22.71, 19.47, 17.40, 14.56, 14.45, 14.26, 14.14, 13.99, 12.11, 11.32. HRMS (ESI): *m/z* calcd for $C_{229}H_{364}N_6O_{24}$ $[M+H]^+$ 3583.7520, found 3583.7556.

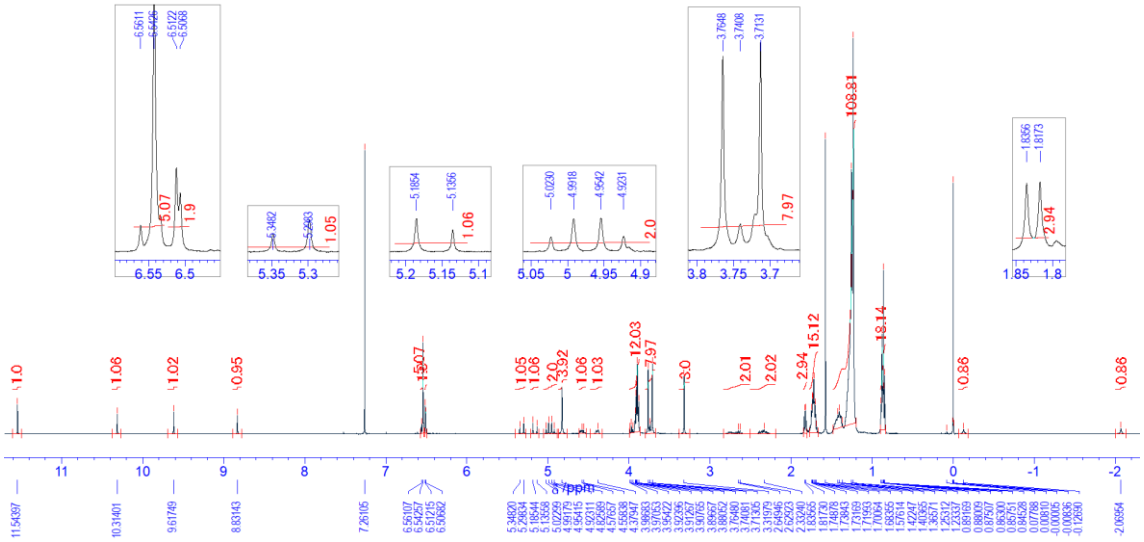

Chart S1 ^{1}H NMR spectrum of compound **4** in $CDCl_3$ at 25 °C.

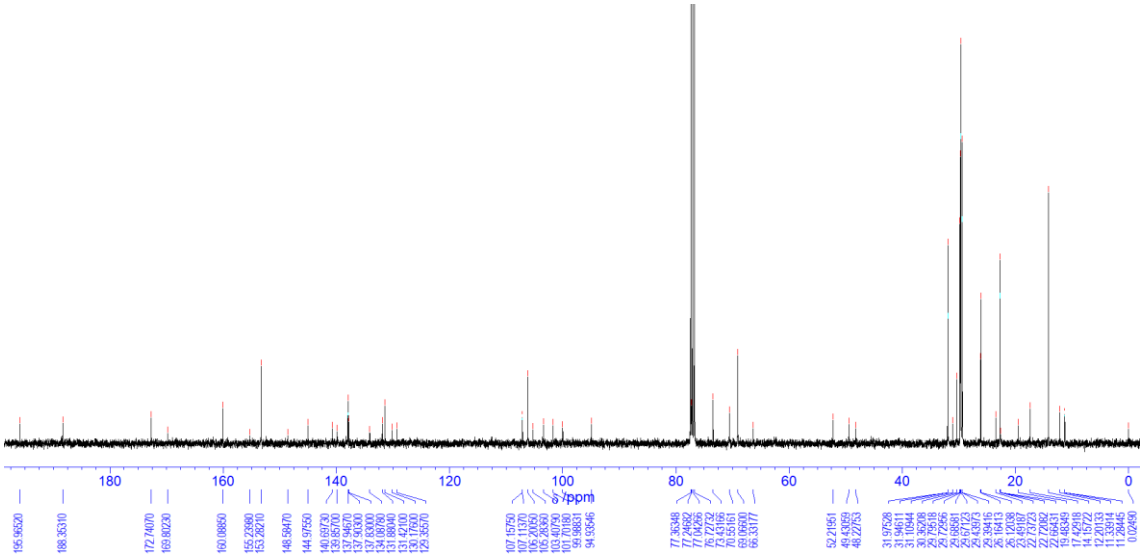

Chart S2 ^{13}C NMR spectrum of compound **4** in $CDCl_3$ at 25 °C.

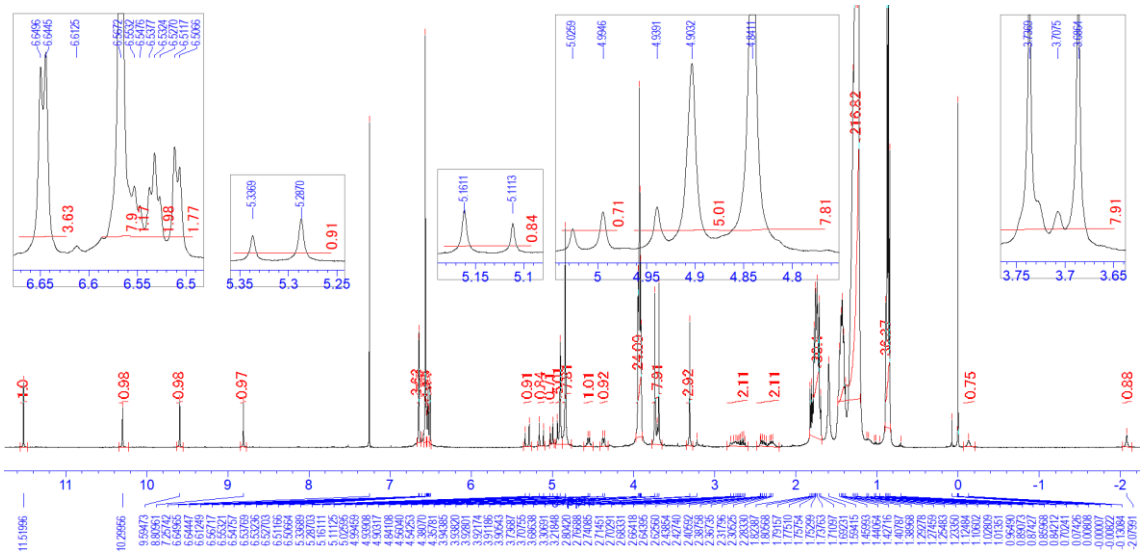

Chart S3 ^{1}H NMR spectrum of compound **5** in $CDCl_3$ at 25 °C.

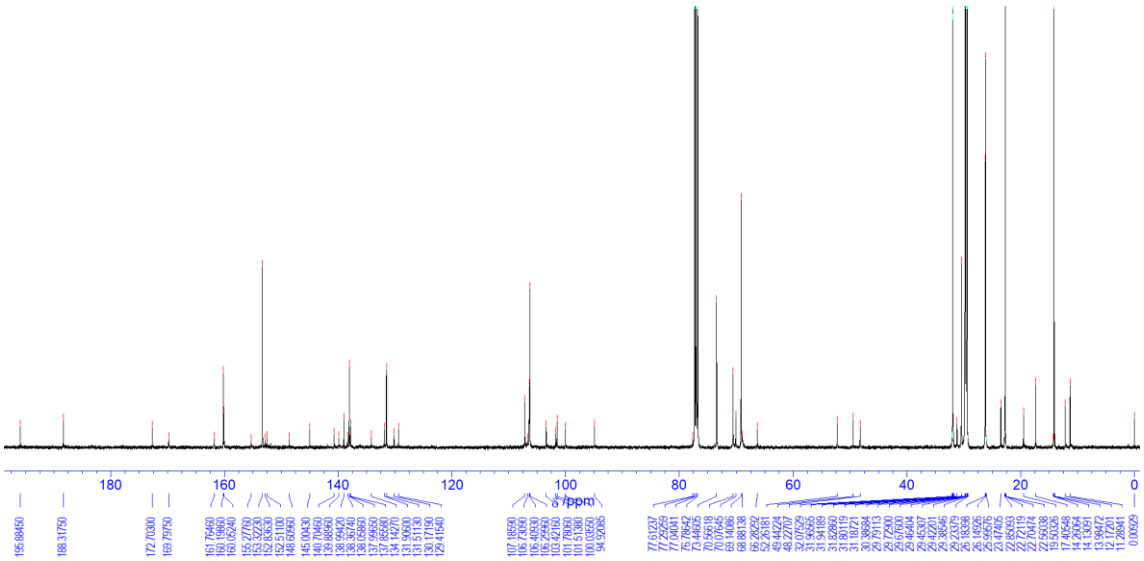

Chart S4 ^{13}C NMR spectrum of compound **5** in $CDCl_3$ at 25 °C.

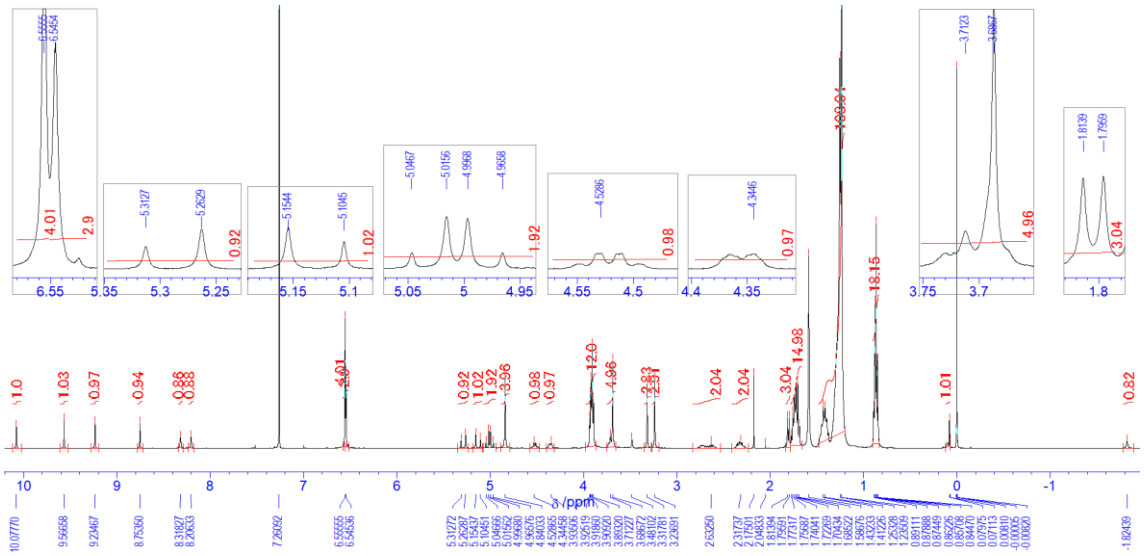

Chart S5 ^{1}H NMR spectrum of **ChG2** in $CDCl_3$ at 25 °C.

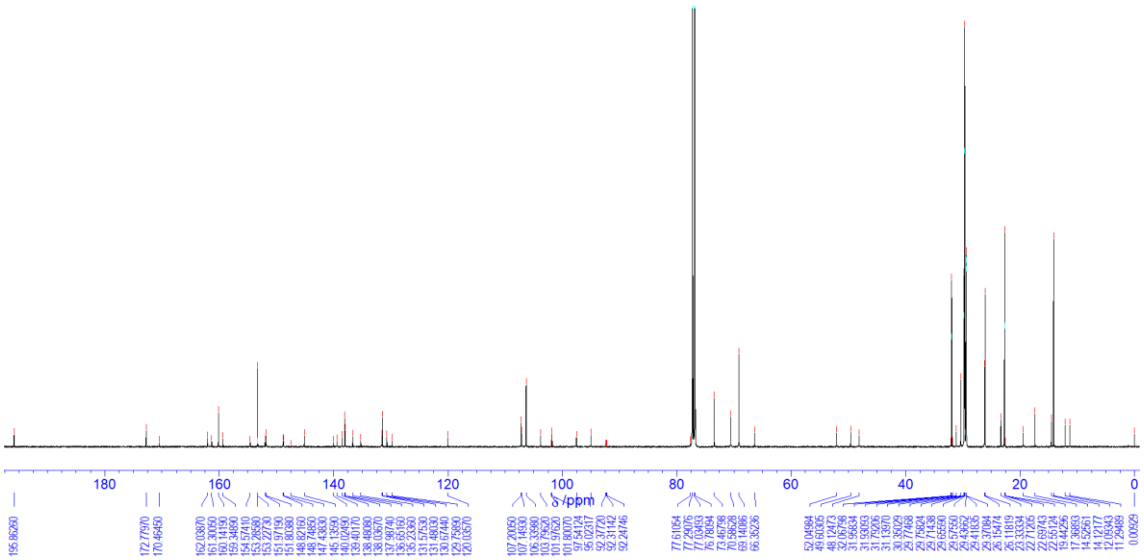

Chart S6 ^{13}C NMR spectrum of **ChG2** in $CDCl_3$ at 25 °C.

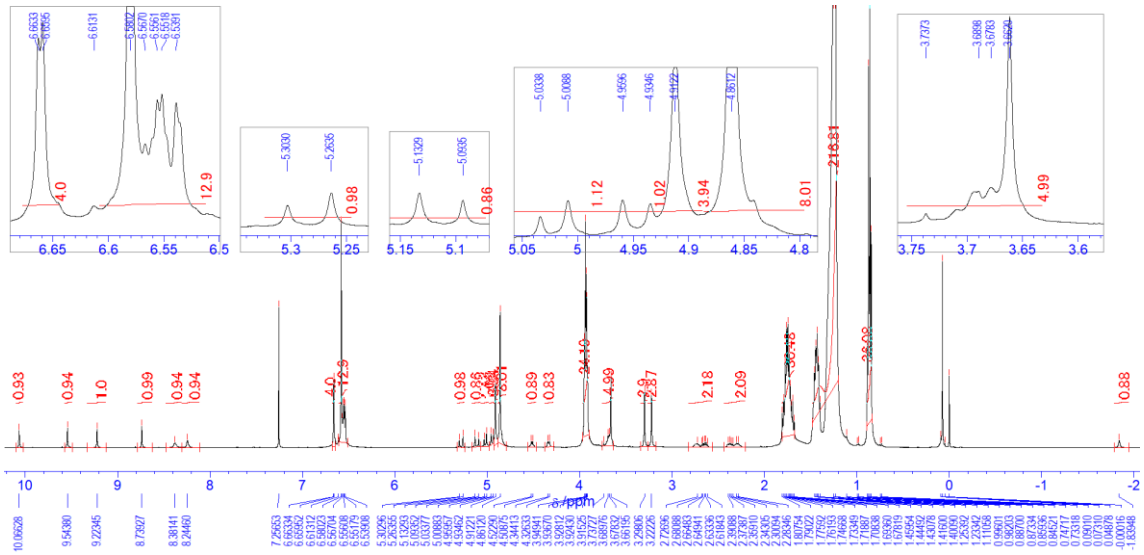

Chart S7 ^{1}H NMR spectrum of **ChG3** in $CDCl_3$ at 25 °C.

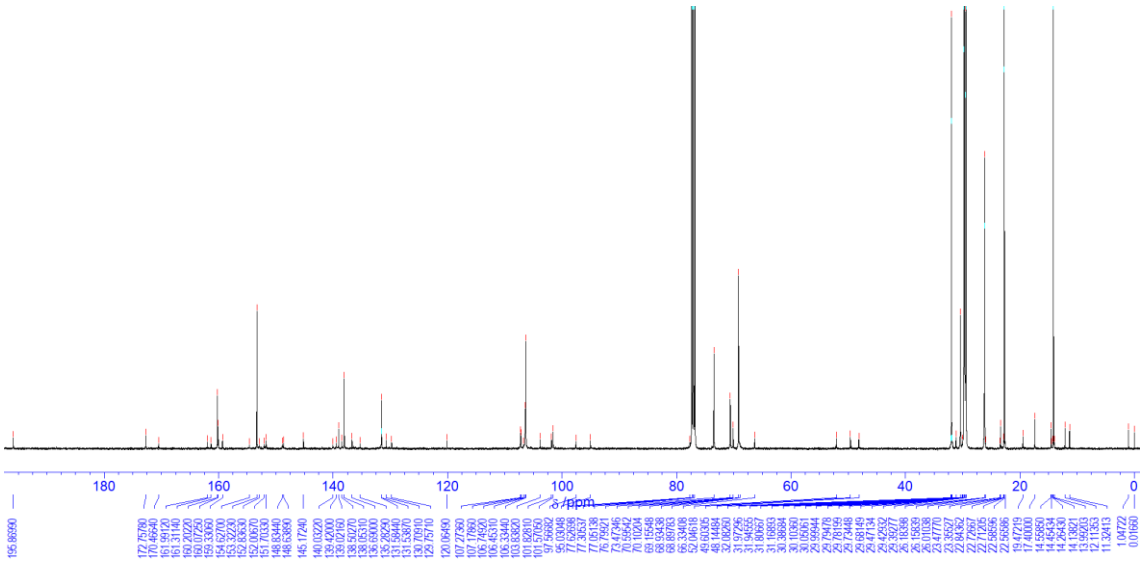

Chart S8 ^{13}C NMR spectrum of **ChG3** in $CDCl_3$ at 25 °C.

3. Supporting Figures

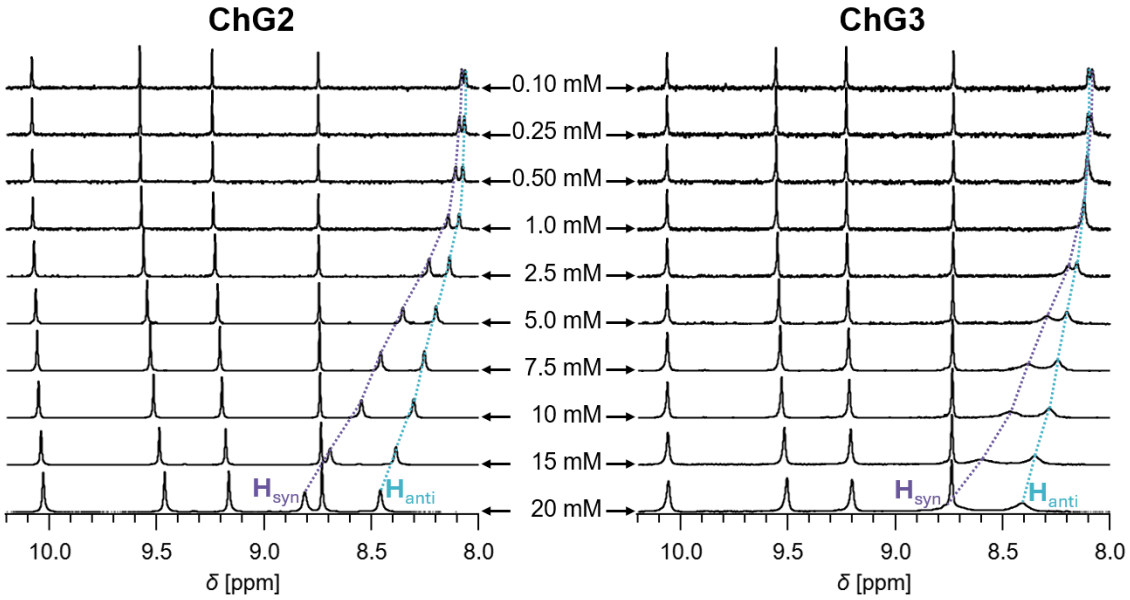

Fig. S1 Concentration-dependent ^{1}H NMR spectra of **ChG2** and **ChG3** in $CDCl_3$ at 25 °C.

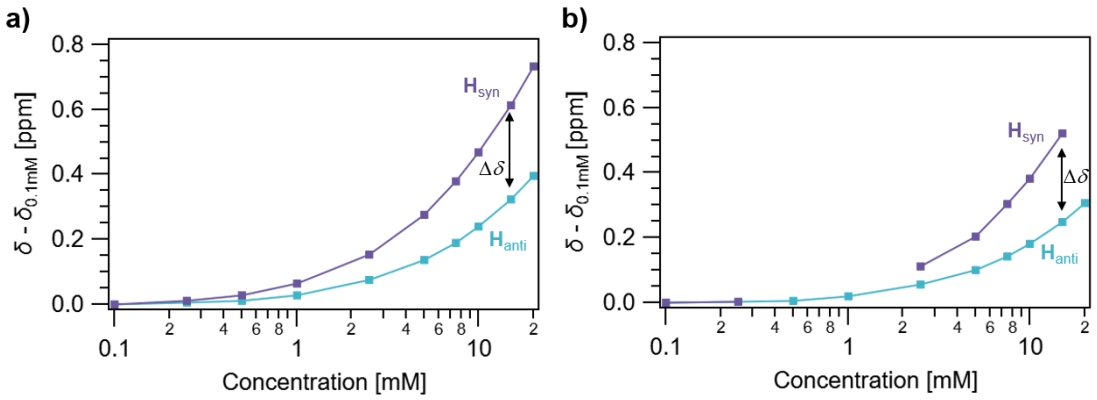

Fig. S2 Concentration-dependent shifts of NH signals ($\delta - \delta_{0.1\mathrm{mM}}$) of a) **ChG2** and b) **ChG3**.

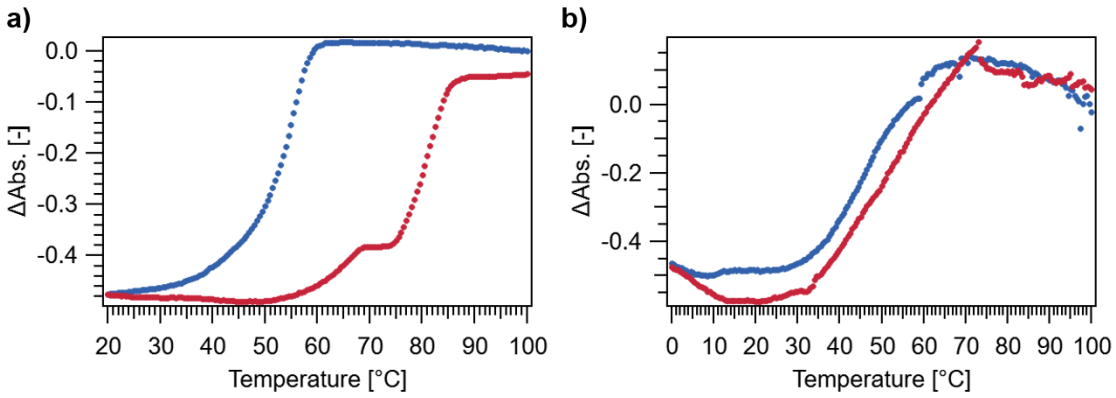

Fig. S3 Cooling (blue) and heating (red) curves of a) **ChG2** (10 μM) and b) **ChG3** (150 μM) obtained by plotting the absorption at 386 nm as a function of temperature.

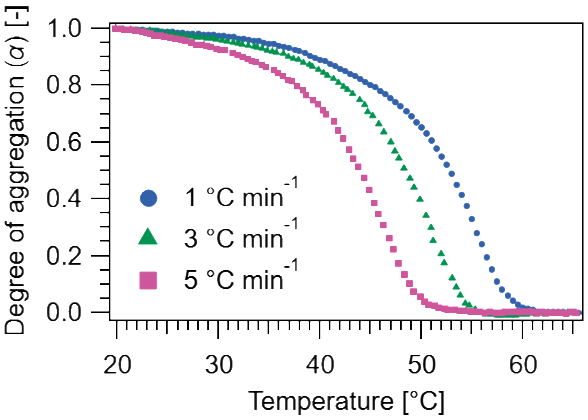

Fig. S4 Cooling curves of **ChG2** (c = 10 μM) with different cooling rate. The curves were obtained by plotting the absorption at 386 nm as a function of temperature.

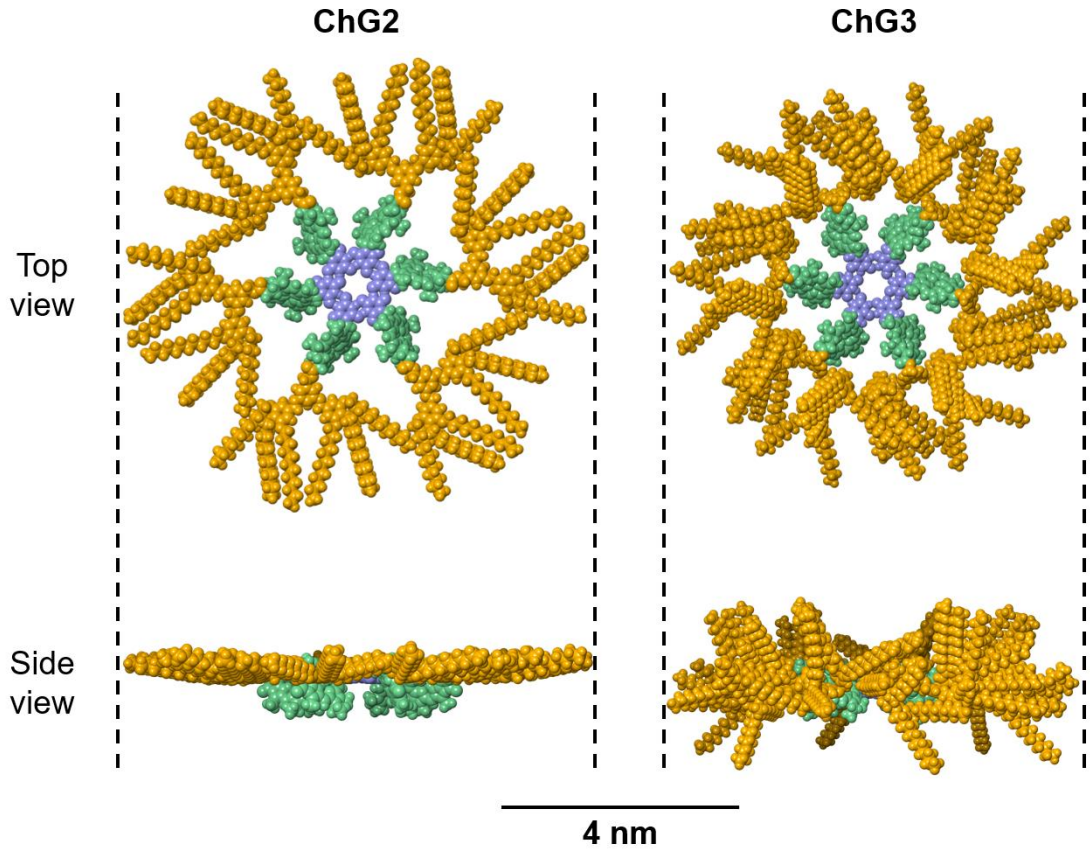

Fig. S5 Molecular modelled structures of **ChG2** and **ChG3** rosettes. To show distinct stacking capabilities of these rosette, alkyl chains were arranged in the same plane as the rosette before structure optimization. For **ChG3** rosette, the alkyl chains were not held in the same plane due to steric crowding.

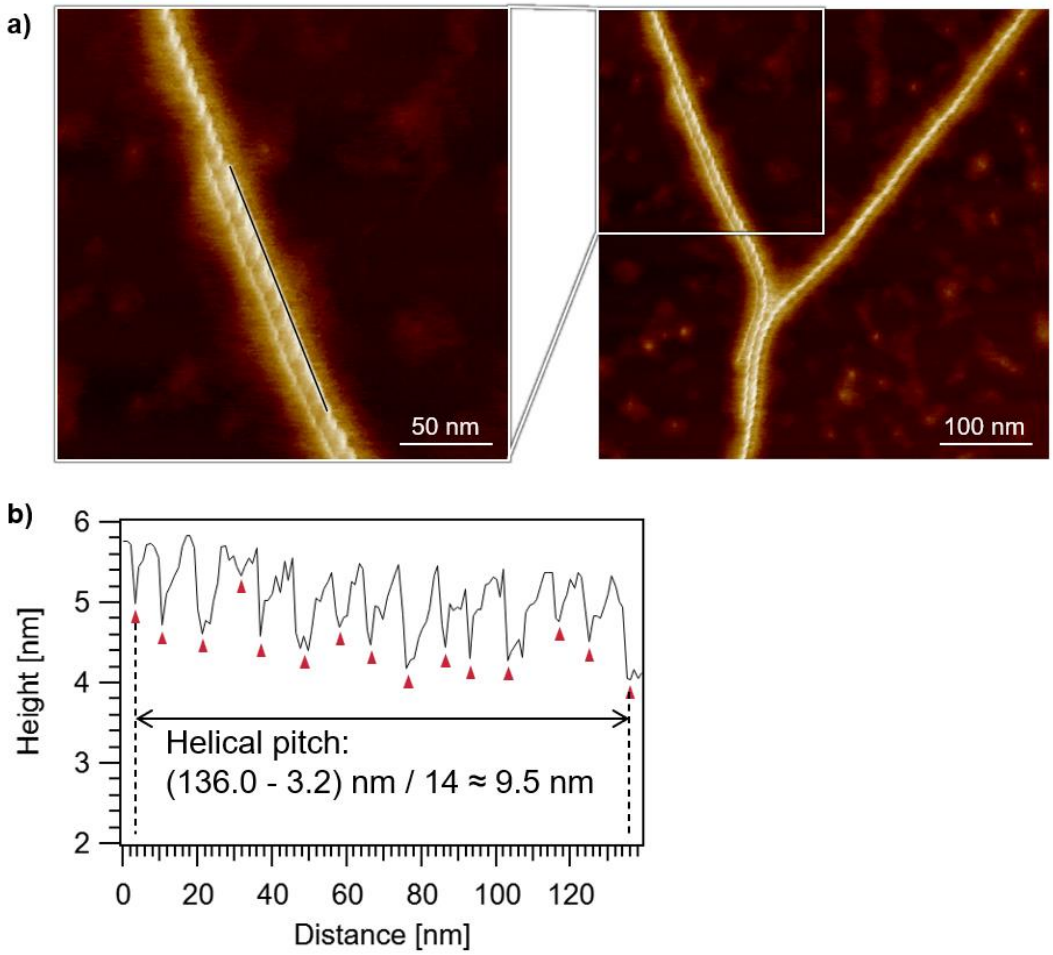

Fig. S6 a) AFM images of nanofibers of **ChG2**. The sample was prepared by spin-coating an MCH solution of **ChG2** (10 μM) immediately after cooling from 100 to 20 °C at a rate of 1 °C/min. b) AFM cross-sectional analysis of a helical nanofiber along the black line in a).

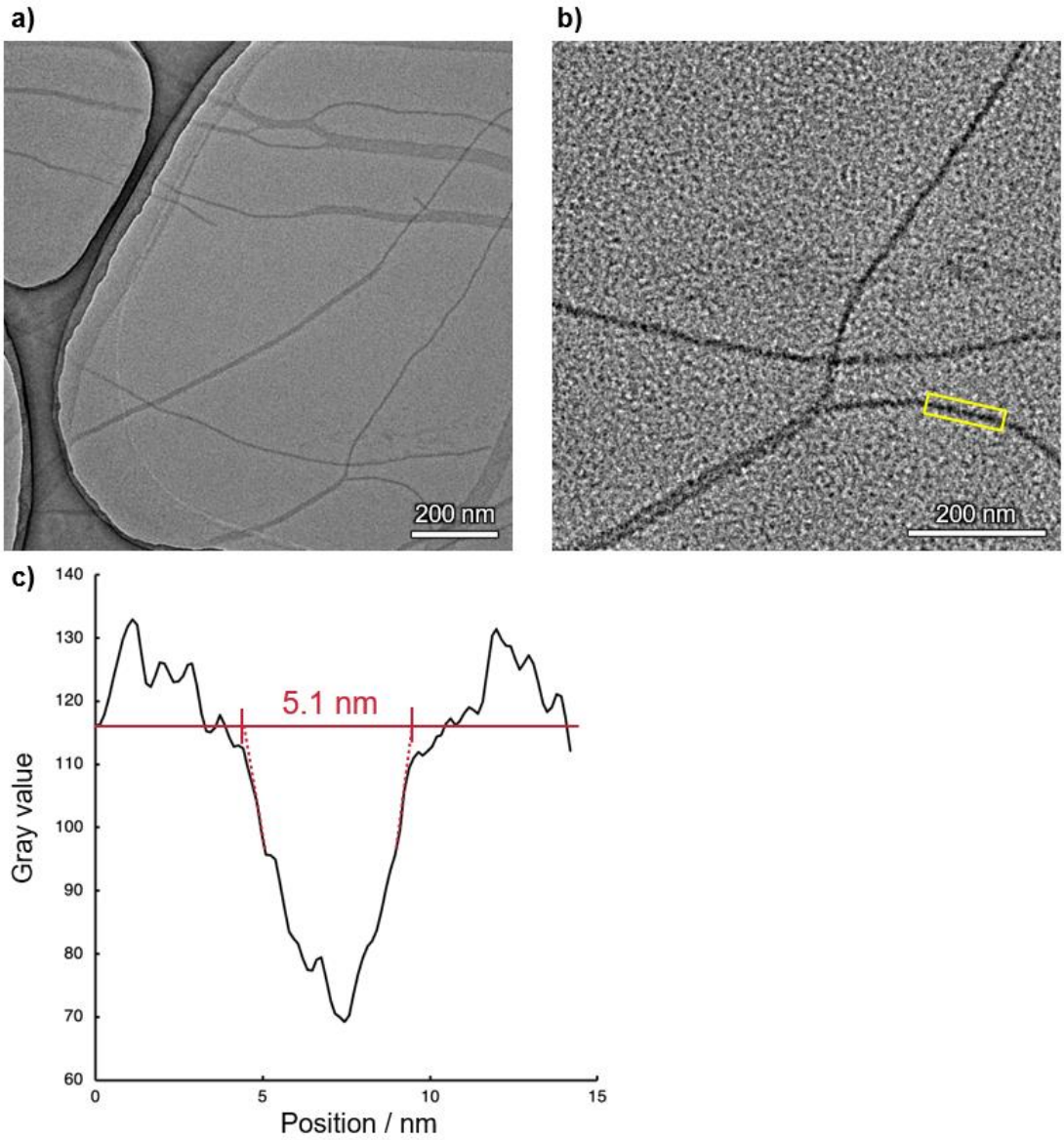

Fig. S7 a,b) TEM images of nanofibers of **ChG2**. The sample was prepared by drop-casting 10 μL of a MCH solution (30 μM) of **ChG2** onto an amorphous carbon film. c) Intensity profile of the area surrounded by yellow box in b). The horizontal red line corresponds to the gray value of the image background.

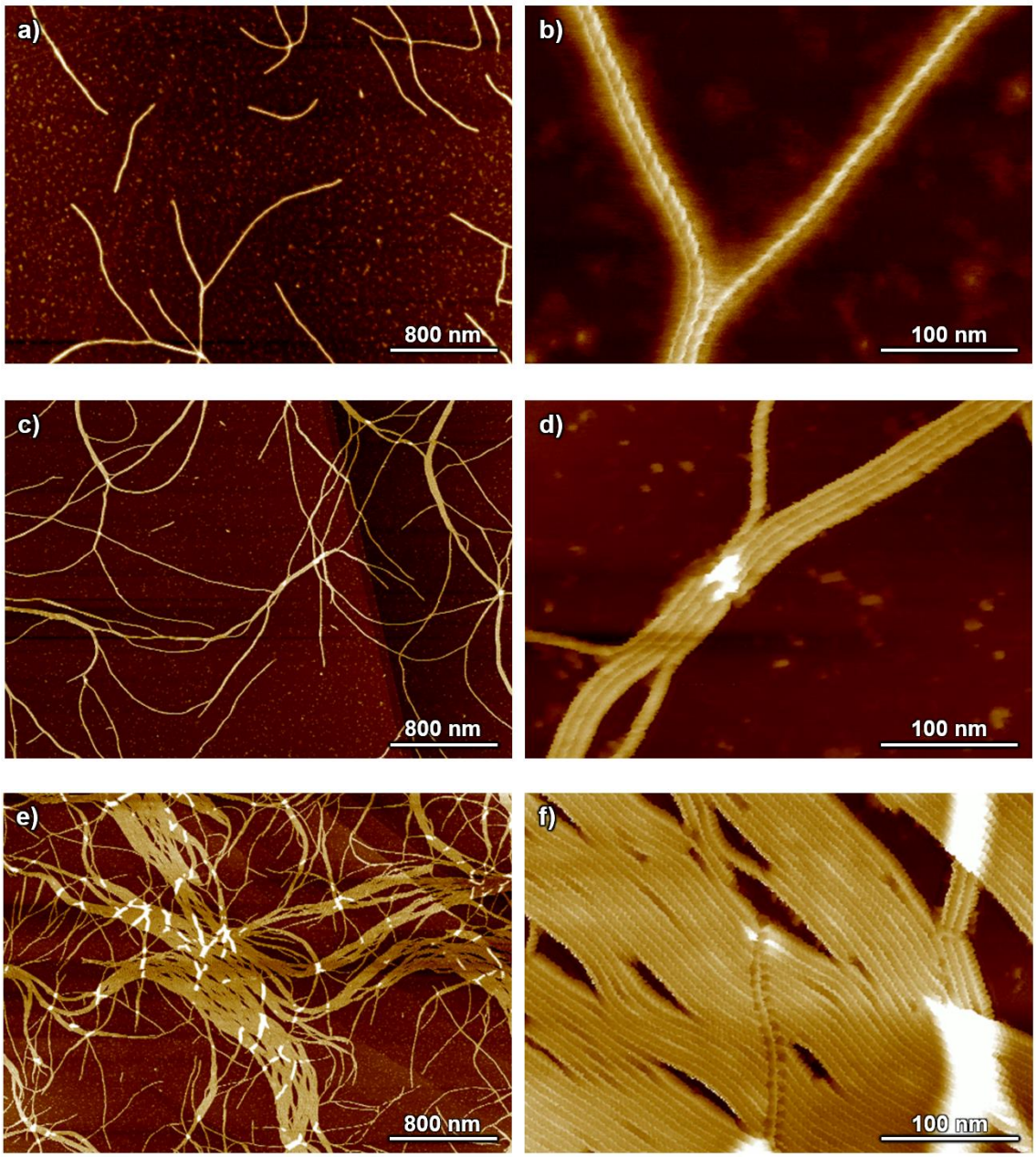

Fig. S8 AFM images of nanofibers of **ChG2** prepared at different concentrations. a,b) 10 μM; c,d) 30 μM; e,f) 150 μM.

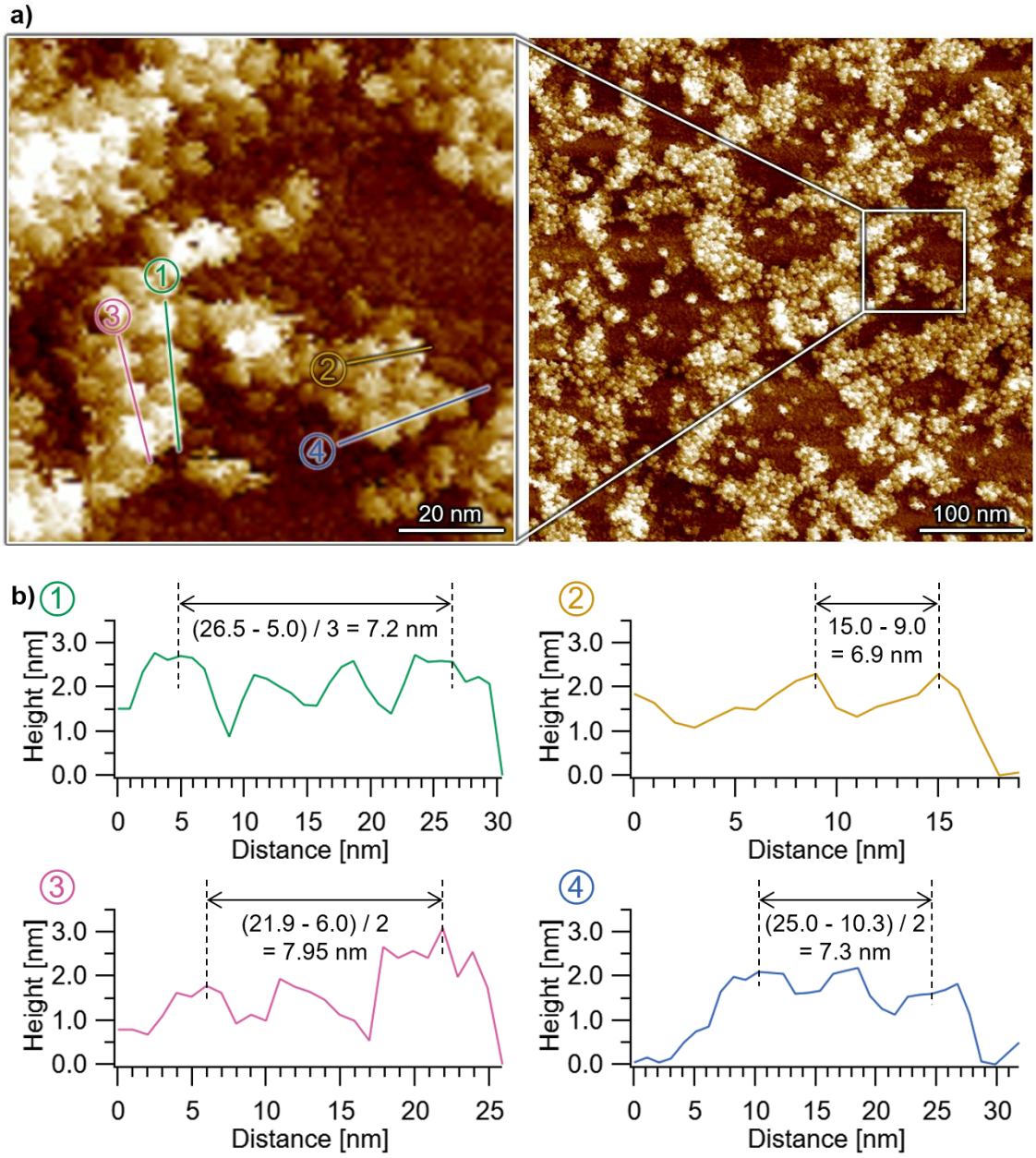

Fig. S9 a) AFM images of nanoparticles of **ChG3**. The sample was prepared by spin-coating an MCH solution of **ChG3** (150 μM) immediately after cooling from 100 to 20 °C at a rate of 1 °C/min. b) AFM cross-sectional analysis of nanoparticles along the lines ①–④ in a).

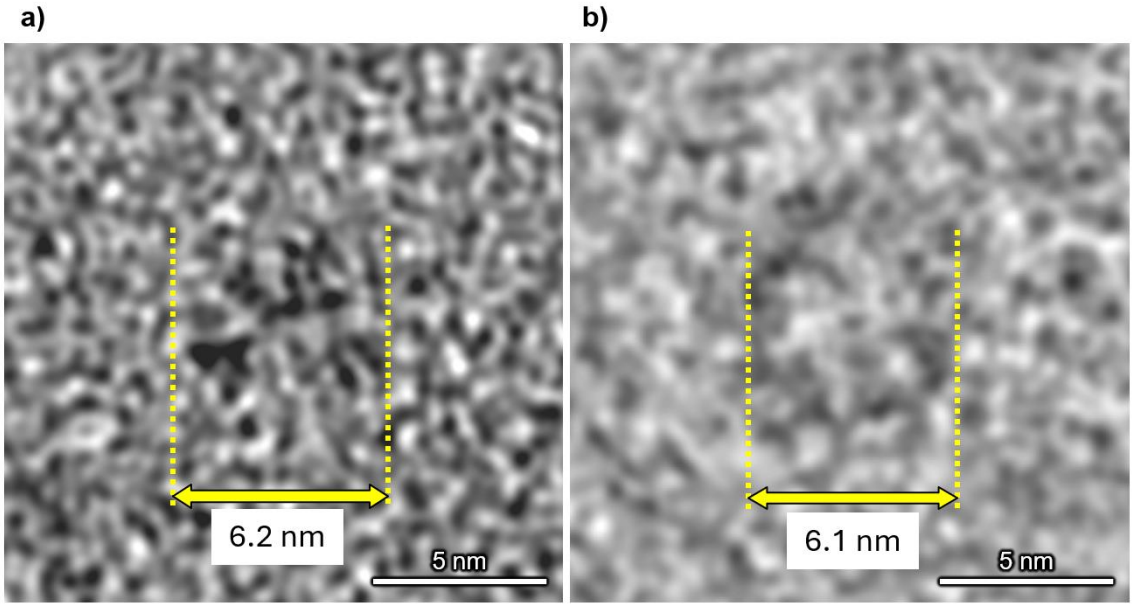

Fig. S10 a) TEM image of a single **ChG3** particle on an amorphous carbon film. b) TEM simulation of a single **ChG3** rosette. Contrast of 6-nm-thick amorphous carbon film is included in the simulated image.

4. Supplementary References

S1 M. D. Abramoff, P. J. Magalhaes, S. J. Ram, Image Processing with ImageJ, *Biophotonics Intern.*, 2004, **11**, 36.

S2 F. Hosokawa, T. Shinkawa, Y. Arai, T. Sannomiya, Benchmark test of accelerated multi-slice simulation by GPGPU, *Ultramicroscopy*, 2015, **158**, 56.

S3 N. Shimizu, K. Yatabe Y. Nagatani, S. Saijyo, T. Kosuge and N. Igarashi, Software development for analysis of small-angle x-ray scattering data, *AIP Conf. Proc.*, 2016, **1741**, 050017.

S4 Mantid 6.9.1: Manipulation and Analysis Toolkit for Instrument Data.; Mantid Project. Doi: 10.5286/Software/Mantid6.9.1; O. Arnold, J. C. Bilheux, J. M. Borreguero, A. Buts, S. I. Campbell, L. Chapon, M. Doucet, N. Draper, R. Ferraz Leal, M. A. Gigg, V. E. Lynch, A. Markvardsen, D. J. Mikkelson, R. L. Mikkelson, R. Miller, K. Palmen, P. Parker, G. Passos, T. G. Perring, P. F. Peterson, S. Ren, M. A. Reuter, A. T. Savici, J. W. Taylor, R. J. Taylor, R. Tolchenov, W. Zhou, J. Zikovsky, Mantid-Data Analysis and Visualization Package for Neutron Scattering and μ-SR Experiments, *Nuclear Instruments and Methods in Physics Research Section A: Accelerators, Spectrometers, Detectors and Associated Equipment*, 2014, **764**, 156. Doi: 10.1016/j.nima.2014.07.029 (download bibtex)

S5 core_shell_bicelle — SasView 5.0.6 documentation, https://www.sasview.org/docs/user/models/core_shell_bicelle.html, (accessed August 2024).

S6 S. Datta, Y. Kato, S. Higashiharaguchi, K. Aratsu, A. Isobe, T. Saito, D. D. Prabhu, Y. Kitamoto, M. J. Hollamby, A. J. Smith, R. Dalgliesh, N. Mahmoudi, L. Pesce, C. Perego, G. M. Pavan and S. Yagai, Software development for analysis of small-angle x-ray scattering data, *Nature*, 2020, **583**, 400.

S7 N. Kosaka and H. Tamiaki, Synthesis of a Novel Cyclic Chlorophyll Hetero-Dyad as a Model Compound for Stacked Chlorophylls Found in Photosynthetic Systems, *Eur. J. Org. Chem.*, 2004, 2325.

S8 V. Percec, W. Cho, G. Ungar and D. J. P. Yeardley, Synthesis and Structural Analysis of Two Constitutional Isomeric Libraries of AB_2-Based Monodendrons and Supramolecular Dendrimers, *J. Am. Chem. Soc.*, 2001, **123**, 1302.